# Optical Spectroscopy of Hydrogen-like Atoms

Bhaskar Mookerji and Charles Herder*
*MIT Department of Physics, 8.13*
(Dated: March 5, 2008)

By performing scanning spectrometry on the hydrogenic spectra of hydrogen, deuterium, and sodium, we explore the validity of the Rydberg equation of atomic spectra and its relevant isotope and fine-structure corrections. The Balmer lines of hydrogen and deuterium are measured; the hydrogen Rydberg constant is interpolated to $R_H = 109660.00 \pm 19.60\text{cm}^{-1}$ and the hydrogen-deuterium isotope effect is measured to $0.52 \pm 0.06$. Fine structure splitting in the 3P and 4P orbitals of sodium are observed at $\Delta\bar{\nu}_{3\text{P}} = 17.12 \pm 0.52 \pm 0.05\text{cm}^{-1}$ and $\Delta\bar{\nu}_{4\text{P}} = 5.60 \pm 0.94\text{cm}^{-1}$ and the effective charge $Z_{\text{eff}}$ for $S$ and $P$ shell electrons is calculated, confirming screening in complex atoms.

## 1. INTRODUCTION

Early 20th Century experimentalists showed that the optical spectra of hydrogenic atoms were characterized by quantized energy levels for bound electrons. Quantization in mathematical models of emission spectra provided a basis for the development of early quantum mechanics.

Using a high-resolution scanning monochromator, we investigate the validity of the Rydberg equation by characterizing the emission spectra of hydrogen, deuterium, and sodium. After determining a monochromator calibration curve from a high-intensity mercury spectrum, we measure the mass-dependent Rydberg constants of hydrogen and deuterium. We then characterize corrections to Rydberg equation from the hydrogen-deuterium isotope shift and sodium fine structure. [**?** ]

## 2. THEORY

Our goal is to investigate the energy spectrum of an atom with atomic number $Z$ and singular valence electron interacting in a Coulomb potential described by:

$$H = \frac{\mathbf{p}^2}{2m} - \frac{Ze^2}{4\pi\epsilon_0}\frac{1}{r}. \tag{1}$$

The bound state eigenvalues correspond to the discrete energy levels in hydrogenic atoms given by the Bohr equation:

$$E_n = -hcR_\infty \frac{Z^2}{n^2} = -\frac{m_e e^4}{2\left(4\pi\epsilon_0\right)^2 \hbar^2}\frac{Z^2}{n^2}, \tag{2}$$

where $n$ is the electron's principal quantum number and $R_\infty$ is the Rydberg constant with value $hcR_\infty = 13.6056923(12)\text{eV}$.

Energy is radiated from the atom when an electron in an excited energy state $n_f$ falls to a lower level $n_i$, thereby emitting a photon with energy equal to the difference of the energies of the two levels. Equating this energy to wavelength $\lambda$ yields the Rydberg equation for an atom:

$$\frac{1}{\lambda} = -R_Z Z^2 \left(\frac{1}{n_i^2} - \frac{1}{n_f^2}\right). \tag{3}$$

The Balmer emissions lines of hydrogen and deuterium are given by transitions from $n_i = 3, 4, 5, \ldots$ to $n_f = 2$.

Equation 1 and 2 assume that the nucleus is a fixed-point center of a spherically symmetric potential. With the finite size and mass of the nucleus, Equation 3 takes into account the center of mass of the electron-nucleus system with the Rydberg constant $R_Z$ proportional to $R_\infty$ by $(1 + m_e/m_Z)^{-1}$, where $m_Z$ is the nuclear mass. The mass dependence of the Rydberg constant is observable in lighter atoms, and the resulting wavelength shifts $\Delta\lambda = \lambda_{\text{H}} - \lambda_{\text{D}}$ between hydrogen and deuterium interpolates the isotope mass ratio.

### 2.1. Hydrogenic Fine Structure

Principle energy levels in hydrogenic atoms split due to angular momenta of electrons. An orbiting valence electron has a magnetic moment $\mu$ and sees a magnetic field $\mathbf{B}$ from an orbiting nucleus in its own reference frame. These magnetic quantities are related to the spin $\mathbf{S}$ and orbital angular momenta $\mathbf{L}$ and contribute a perturbation term to Equation 1:

$$H_1 = -\mu \cdot \mathbf{B} = \left(\frac{e^2}{8\pi\epsilon_0}\right)\frac{1}{m^2c^2r^3}\mathbf{S}\cdot\mathbf{L}. \tag{4}$$

The spin-orbit coupled Hamiltonian commutes with $L^2$, $S^2$, and total angular momentum $\mathbf{J} = \mathbf{L} + \mathbf{S}$. Equating the coupling term to these observables and taking the first-order perturbation shows that fine structure states are no longer degenerate for quantum numbers $n$ and $j$:

$$E_{nj} = -\frac{E_n}{n^2}\left[1 + \frac{\alpha^2}{n^2}\left(\frac{n}{j+1/2} - \frac{3}{4}\right)\right]. \tag{5}$$

Furthermore, the probability of a transition occurring between states $|njm\rangle$ is proportional to the matrix elements of a time oscillating electric dipole given by $\langle n'j'm'|\, e\mathbf{r}\,|njm\rangle$, which is only non-zero when $\Delta j = \pm 1$.

*Electronic address: mookerji@mit.edu, cherder@mit.edu

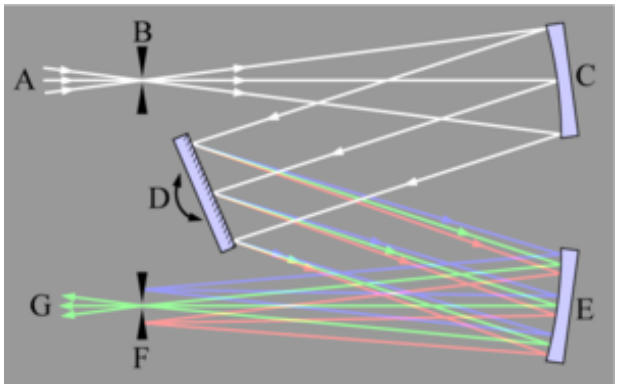


FIG. 1: Czerny-Turner monochromator. (A) Emission source, (B) entrance slit, (C) collimating mirror, (D) diffraction grating, (E) focusing mirror, (F) exit slit, (G) photomultiplier tube.[a]

[a]http://www.answers.com/topic/czerny-turner-png under GPL

## 3. EXPERIMENTAL SETUP AND PROCEDURE

The monochromator setup in this experiment is depicted in Figure 1. A glass lamp is focused at the input slit of a LabView-controlled John Yvon 1250M Czerny-Turner monochromator and photons emitted from electron excitations pass through the slit and are focused by a concave mirror onto a mechanically-adjustable diffraction grating. The diffracted light is then focused by another concave mirror and passed through the exit slit to be measured by a photomultiplier tube (PMT) set at 950V. We determine the wavelengths of emitted photons by mechanically rotating the diffraction grating through a range of angles and measuring the PMT signal calculated by LabView. We minimized ambient light by executing the experiment in complete darkness under a light curtain.

Adjustable monochromator parameters affecting the observed peak resolution and intensity were the entrance/exit slit width, density of the diffraction grating, and source-entrance slit distance. To optimize resolution and line shape, high-intensity peaks were typically measured with 10$\mu$m slit widths and 100ms PMT integration times, whereas peaks with low signal-noise ratio were measured with higher slit widths (20-50$\mu$m) and integration times (200-1000ms). High resolution spectra (3600gvs/mm) were resolved at 0.06Å and low resolution spectra (1800gvs/mm) were resolved between 0.10-0.15Å, however fine spectra were mechanically limited to 5000Å. Therefore, hydrogen and deuterium Balmer spectra were measured using both the 1800gvs/mm and 3600gvs/mm diffraction gratings. Fine structure splitting in sodium were resolved with the 1800gvs/mm grating, as most doublets were outside the mechanical limit of the finer grating. Systematic errors from these parameters are further discussed in Section 4.

Finally, measured hydrogen, deuterium, and sodium spectra are determined after monochromator error was calibrated for using a mercury pen lamp. A rough scan

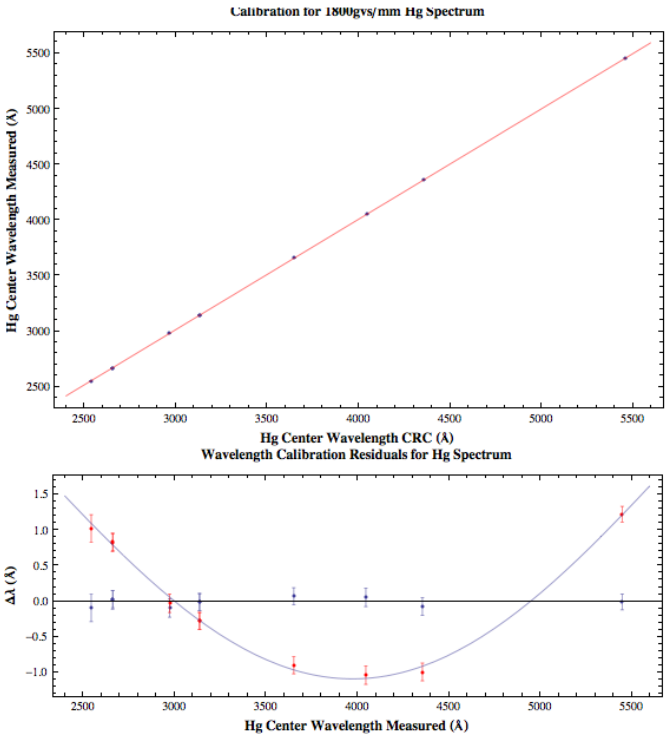


FIG. 2: 1800gvs/mm grating Hg calibration line and residuals. Correlated residuals (red) are error-corrected by a grating term, yielding qualitatively random residuals (blue).

over a few Angstrom wide region allowed us to subsequently focus and well-characterize peaks using both the 1800gvs/mm and 3600gvs/mm gratings with a 0.01Å step size. High-intensity spectral lines of mercury were identified and measured center wavelengths were plotted against accepted CRC values to determine the calibration curve found in Figure 2, as example. A similar procedure was followed for the desired spectra, and the resulting error in calibration is discussed in Section 4.

## 4. RESULTS AND ERROR ANALYSIS

Our peaks were well-approximated by Gaussian distributions with minimally Lorentzian tails, from which center wavelengths and full width at half maximum (FWHM) could be calculated accounting for monochromator background noise with mean 210 counts/sec and 45 counts/sec deviation.

The systematic errors from finite entrance/exit slit width, grating resolution, natural line width, and Doppler broadening add in quadrature to equal the FWHM determined from a given data set. Slit error predominates error from line width and Doppler broadening ($\Delta\lambda \leq 0.001$Å for $T = 2700$K lamp and $Z = 11$). Standard Gaussian error is scaled to FWHM by $\sigma_{\mathrm{FWHM}} = \Delta\lambda_{\mathrm{FWHM}}/\sqrt{2\ln 2}$ and added in quadrature to calibration error for total error in wavelength.

TABLE I: Classification of hydrogen Balmer transitions and deuterium wavelength shifts to $n_f = 2$ (in air).

| | CRC | | 1800gvs/mm | | 3600gvs/mm | |
|---|---|---|---|---|---|---|
| Transition | $\lambda$ | $\Delta\lambda$ | $\lambda$ | $\Delta\lambda$ | $\lambda$ | $\Delta\lambda$ |
| $H_\alpha\,(n_i = 3)$ | 6562.85 | 1.79 | $6539.54 \pm .0003$ | $1.72 \pm 0.06$ | – | – |
| | 6562.72 | | $6539.39 \pm .0003$ | | – | – |
| $H_\beta\,(n_i = 4)$ | 4861.33 | 1.32 | $4861.4 \pm 0.20$ | $1.22 \pm 0.08$ | $4861.5 \pm 0.19$ | $1.29 \pm 0.03$ |
| $H_\gamma\,(n_i = 5)$ | 4340.47 | 1.18 | $4340.5 \pm 0.22$ | $1.10 \pm 0.07$ | $4340.5 \pm 0.16$ | $1.16 \pm 0.03$ |
| $H_\delta\,(n_i = 6)$ | 4101.74 | 1.12 | $4101.8 \pm 0.18$ | $1.04 \pm 0.09$ | $4101.8 \pm 0.17$ | $1.09 \pm 0.03$ |
| $H_\epsilon\,(n_i = 7)$ | 3970.07 | 1.08 | $3970.2 \pm 0.22$ | $1.02 \pm 0.09$ | $3970.1 \pm 0.16$ | $1.06 \pm 0.03$ |
| $H_\zeta\,(n_i = 8)$ | 3889.05 | 1.05 | $3889.2 \pm 0.24$ | $1.03 \pm 0.10$ | n/a | n/a |
| $H_\eta\,(n_i = 9)$ | 3835.39 | 1.04 | $3835.5 \pm 0.46$ | $1.07 \pm 0.20$ | n/a | n/a |

[a] n/a: Point lost or unmeasured.

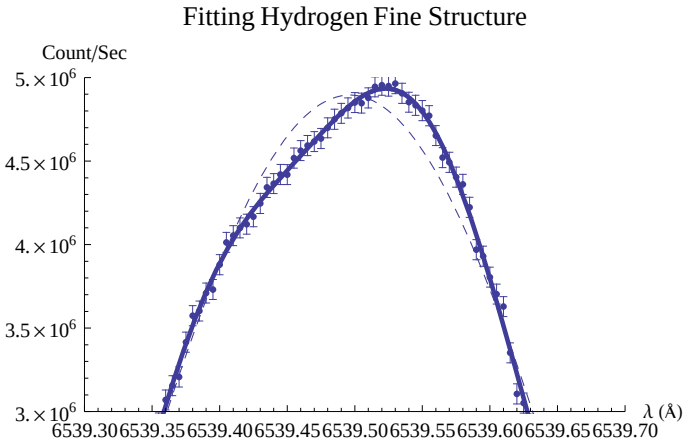


FIG. 3: Unresolved fine structure splitting of $H_\alpha$ by 1800gvs/mm grating. Double (think curve—93% confidence) and single Gaussian (thin curve—$10^{-76}$% confidence) models are plotted against unresolved fine structure splitting.

### 4.1. Mercury Calibration

For calibration, we scanned 10 peaks in the first-order mercury spectrum from 2536.52–5460.74Å using the 1800gvs/mm and 3600gvs/mm gratings. The residuals of the 3600gvs/mm calibration indicated a strictly linear calibration, as the monochromator compensates well for non-linearity in the middle of the diffraction grating's free spectral range. However, the 1800gvs/mm calibration curve in Figure 2 shows correlated residuals when using a strictly fit to our data. This non-linearly is related to the grating equation describing the diffraction in the spectrometer that separates spectral lines. Subsequently, this systematic error is compensated for through a non-linear, first-order sinusoidal fit that well-compensated for our experimental error, thereby resulting in qualitatively random residuals (Figure 2). Uncalibrated measured wavelengths were adjusted by applying an numerical root-finder in Mathematica to our calibration curve. The standard error $\sigma_{\text{Calib.}}$ on the 1800gvs/mm and 3600gvs/mm were 0.06Å(98% confidence) and 0.05Å(95% confidence), respectively.

### 4.2. Rydberg Constant of Hydrogen and Isotope Mass Ratio

Using a combined hydrogen-deuterium gas lamp, we measured spectral lines in the Balmer series for hydrogen and deuterium using both the 1800gvs/mm and 3600gvs/mm grating and list them in Table I. Mechanically limited or UV-filtered spectra could not be measured. The raw data of these spectra and their isotope shifts are given in Table I, and wavelengths used in model fitting were corrected by the index of refraction of air ($n_{\text{air}} = 1.00027$). Plotting wavelength against principle quantum number using Equation 3 as linear model, we determine $R_H = 109690.00 \pm 19.80\text{cm}^{-1}$ $\left(\chi^2 = 0.2\right)$ for the 1800gvs/mm grating and $R_H = 109660.00 \pm 19.60\text{cm}^{-1}$ $\left(\chi^2 = 0.32\right)$ for the 3600gvs/mm grating. This agrees within experimental error and excellent confidence with the accepted CRC value $R_H = 109677.58341 \pm 0.00001\text{cm}^{-1}$ with 99% and 98% confidence, respectively.

Using a 4$\mu$m slit width and long integration time, the $H_\alpha$ fine structure splitting was measured to $0.150 \pm 0.007$Å within experimental error of the accepted value 0.157Å. Resolving the peak was beyond the resolution the grating and the monochromator, but wavelengths of two centered, overlapping Gaussians was calculated a Marquandt non-linear fitting algorithm implemented in Mathematica (Figure 3).

From the mass-dependent isotope shifts of the Rydberg constant in Equation 3, we plot the difference of atomic H and D Rydberg equations, and use the slope of a fit line to determine the $m_{\text{H}}/m_{\text{D}}$ to $0.50 \pm 0.06$ $\left(\chi^2 = 0.2\right)$ and $0.52 \pm 0.06$ $\left(\chi^2 = 0.32\right)$ for the 1800gvs/mm and 3600gvs/mm, respectively. Therefore mass ratio was measured within experimental error with 99% confidence.

### 4.3. Fine Structure of Sodium

Within the mechanical limits of the monochromator, we successfully identified eight allowed 3P transitions in the first-order spectrum of sodium, in addition to a sin-

TABLE II: Classification of sodium fine structure.

| | CRC | 1800gvs/mm | |
|---|---|---|---|
| Transition | $\lambda$(Å) | $\lambda$(Å) | $\Delta\bar{\nu}$(cm$^{-1}$) |
| $5S \rightarrow 3P_{3/2}$ | 6160.75 | $6159.65 \pm 0.25$ | $14.65 \pm 0.40$ |
| $\rightarrow 3P_{1/2}$ | 6154.23 | $6154.09 \pm 0.20$ | |
| $3P_{3/2} \rightarrow 3S$ | 5895.92 | $5895.77 \pm 0.13$ | $17.25 \pm 0.28$ |
| $3P_{1/2} \rightarrow 3S$ | 5889.95 | $5889.78 \pm 0.13$ | |
| $4D \rightarrow 3P_{3/2}$ | 5688.21 | $5688.25 \pm 0.12$ | $17.43 \pm 0.29$ |
| $\rightarrow 3P_{1/2}$ | 5682.63 | $5682.61 \pm 0.12$ | |
| $6S \rightarrow 3P_{3/2}$ | 5153.40 | $5153.58 \pm 0.16$ | $17.17 \pm 0.41$ |
| $\rightarrow 3P_{1/2}$ | 5148.84 | $5149.03 \pm 0.14$ | |
| $5D \rightarrow 3P_{3/2}$ | 4982.81 | $4983.11 \pm 0.15$ | $17.12 \pm 0.44$ |
| $\rightarrow 3P_{1/2}$ | 4978.54 | $4978.86 \pm 0.16$ | |
| $7S \rightarrow 3P_{3/2}$ | 4751.82 | $4752.09 \pm 0.22$ | $17.32 \pm 0.61$ |
| $\rightarrow 3P_{1/2}$ | 4749.94 | $4748.18 \pm 0.20$ | |
| $6D \rightarrow 3P_{3/2}$ | 4668.56 | $4668.77 \pm 0.16$ | $17.32 \pm 0.51$ |
| $\rightarrow 3P_{1/2}$ | 4664.81 | $4665.00 \pm 0.15$ | |
| $7D \rightarrow 3P_{3/2}$ | 4497.66 | $4497.89 \pm 0.27$ | $17.00 \pm 0.90$ |
| $\rightarrow 3P_{1/2}$ | 4494.18 | $4494.45 \pm 0.31$ | |
| $4P_{3/2} \rightarrow 3S$ | 3302.98 | $3303.26 \pm 0.14$ | $5.60 \pm 0.94$ |
| $4P_{1/2} \rightarrow 3S$ | 3302.37 | $3302.64 \pm 0.14$ | |
| $5P_{3/2} \rightarrow 3S$ | 2853.01 | – | – |
| $5P_{1/2} \rightarrow 3S$ | 2852.81 | – | |

gle 4P transition (Table II). Transitions only occurred between adjacent angular momentum states, confirming the selection rule $\Delta j = \pm 1$. The 5P transitions were not measured due to UV attenuation in the glass of the sodium lamp.

Doublet separations are given in wavenumbers $\Delta\bar{\nu}$, where $\bar{\nu} = 1/\lambda$. Propagating errors in terms of measured wavelengths and associated errors is given by:

$$\sigma^2_{\Delta\bar{\nu}} = \frac{\sigma^2_{\lambda_1}}{\lambda_1^4} + \frac{\sigma^2_{\lambda_2}}{\lambda_2^4} \tag{6}$$

NIST values for the doublet separations are given by $\Delta\bar{\nu}_{4P} = 5.59\text{cm}^{-1}$ and $\Delta\bar{\nu}_{3P} = 17.196\text{cm}^{-1}$; our aggregated splitting are given by $\Delta\bar{\nu}_{3P} = 17.12 \pm 0.52 \pm 0.05\text{cm}^{-1}$ and $\Delta\bar{\nu}_{4P} = 5.60 \pm 0.94\text{cm}^{-1}$. Individual 3P and 4P doublets largely agree with accepted values within some experimental error. A ratio of the splittings confirm that fine structure splitting decreases dramatically for increases in principle quantum numbers. However, these do not decrease as $1/n^3$, but more like $\text{Log}_{\frac{4}{3}}[\Delta\bar{\nu}_{3P}/\Delta\bar{\nu}_{4P}] = 3.88$, which would agree with the theoretically calculated value of 3.90. From the small size of our sample set, we cannot empirically determine if a power-law describes this energy scaling.

### 4.4. Screening Charge

A consequence of non-degenerate angular momenta $l$ for electrons is the inner-shell electron screening of proton charge $Ze$ seen by valence electrons. Instead, valence electrons see a reduced central charge $Z_{\text{eff}}e$. Those with lower angular momenta $l$ are, on average, closer to the nucleus and experience a greater effective charge. For sodium ($Z = 11$), $Z_{\text{eff}}$ is approximately 1.1456 and 1 for the $S$ and $D$ electrons, respectively.

Measuring $Z_{\text{eff}}$ from our sodium data requires ignoring fine structure effects on the order of $\alpha^2 mc^2$ and equating doublets with a common intermediate state. Assuming that $Z_{\text{eff}}$ differs for $S$ and $P$ orbitals, the Rydberg equation for the $|nlm\rangle_{i\rightarrow f}$ transition is

$$\frac{1}{\lambda} = -R_{\text{Na}}\left(\frac{Z^2_{\text{eff}_i}}{n_i^2} - \frac{Z^2_{\text{eff}_f}}{n_f^2}\right). \tag{7}$$

The solution to two Rydberg equations equating different principle energy levels but identical momenta is given by

$$\frac{1}{\lambda_f} \pm^s_d \frac{1}{\lambda_i} = -Z^2_{\text{eff}} R_{\text{Na}}\left(\frac{1}{n_i^2} - \frac{1}{n_f^2}\right), \tag{8}$$

where the dipole selection rule $\Delta j = \pm 1$ results in a sign difference for the fit equations for $Z_s$ and $Z_d$.

Our measured $Z_s = 1.50 \pm 0.10$ and $Z_d = 1.00 \pm 0.09$ are significantly smaller than the nucleus charge $Z = 11$, confirming the validity of screening from angular momentum and the relative effective charge of $S$ and $D$ electrons. With the $3S$ electron, we also calculate the first ionization energy of sodium to $IE_1 = 7.65 \pm 0.03$eV. The NIST value is given by 5.1391eV.

## 5. CONCLUSIONS

In summary, we have measured the elements of the first order spectrum of hydrogen, deuterium, and sodium and associated fine structure corrections. From these spectra, we determined the mass-dependent Rydberg constants of hydrogen and deuterium and calculated their isotope mass ratio to within experimental error of published values. Sodium fine spectra were largely within experimental error, and $4P$ and $3P$ doublet separations confirmed a power-law dependence on doublet separations and screening of valence electrons in complex hydrogenic atoms.

### Acknowledgments

B. Mookerji thanks C. Herder for his equal contribution to the this experiment and its analysis, and the Junior Lab staff.